HOKKAIDO UNIVERSITY

Title	Signal pulse emulation for scintillation detectors using Geant4 Monte Carlo with light tracking simulation
Author(s)	Ogawara, R.; Ishikawa, M.
Citation	Review of Scientific Instruments, 87(7), 075114 https://doi.org/10.1063/1.4959186
Issue Date	2016-07
Doc URL	http://hdl.handle.net/2115/66891
Rights	This article may be downloaded for personal use only. Any other use requires prior permission of the author and AIP Publishing. The following article appeared in Review of Scientific Instruments and may be found at http://scitation.aip.org/content/aip/journal/rsi/87/7/10.1063/1.4959186. Copyright 2016 Author(s). This article is distributed under a Creative Commons Attribution http://creativecommons.org/licenses/by/4.0/ License.
Rights(URL)	http://creativecommons.org/licenses/by/4.0/
Type	article
File Information	Rev Sci Instrum_87(7)_075114.pdf

Instructions for use

Hokkaido University Collection of Scholarly and Academic Papers : HUSCAP

AIP | Review of Scientific Instruments

Signal pulse emulation for scintillation detectors using Geant4 Monte Carlo with light tracking simulation

R. Ogawara and M. Ishikawa

Citation: Review of Scientific Instruments **87**, 075114 (2016); doi: 10.1063/1.4959186
View online: http://dx.doi.org/10.1063/1.4959186
View Table of Contents: http://scitation.aip.org/content/aip/journal/rsi/87/7?ver=pdfcov
Published by the AIP Publishing

Articles you may be interested in

Web-based, GPU-accelerated, Monte Carlo simulation and visualization of indirect radiation imaging detector performance
Med. Phys. **41**, 121907 (2014); 10.1118/1.4901516

Rapid Monte Carlo simulation of detector DQE(f)
Med. Phys. **41**, 031916 (2014); 10.1118/1.4865761

Monte Carlo code G3sim for simulation of plastic scintillator detectors with wavelength shifter fiber readout
Rev. Sci. Instrum. **83**, 043301 (2012); 10.1063/1.3698089

Experimental validation of Monte Carlo (MANTIS) simulated x-ray response of columnar CsI scintillator screens
Med. Phys. **36**, 4944 (2009); 10.1118/1.3233683

Scintillator Detectors for Scanning Transmission X-ray Microscopes at the Advanced Light Source
AIP Conf. Proc. **705**, 973 (2004); 10.1063/1.1757959

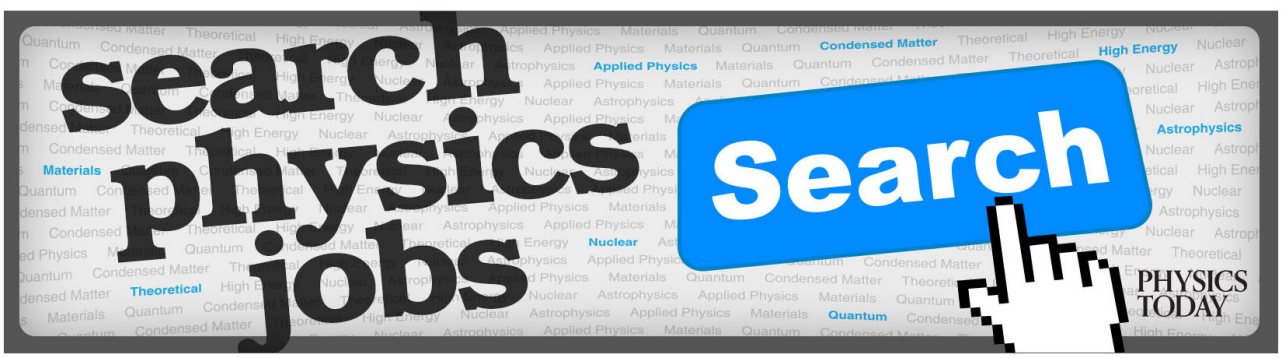

Reuse of AIP Publishing content is subject to the terms at: https://publishing.aip.org/authors/rights-and-permissions. Download to IP: 133.87.84.66 On: Tue, 02 Aug 2016 05:42:11

Signal pulse emulation for scintillation detectors using Geant4 Monte Carlo with light tracking simulation

R. Ogawara[1] and M. Ishikawa[2,a)]
[1]*Department of Medical Physics and Engineering, Graduate School of Medicine, Hokkaido University, Kita-15 Nishi-7, Kita-ku, Sapporo-shi, Hokkaido, Japan*
[2]*Graduate School of Health Science, Hokkaido University, Kita-12 Nishi-5, Kita-ku, Sapporo-shi, Hokkaido, Japan*

(Received 18 May 2016; accepted 8 July 2016; published online 22 July 2016)

The anode pulse of a photomultiplier tube (PMT) coupled with a scintillator is used for pulse shape discrimination (PSD) analysis. We have developed a novel emulation technique for the PMT anode pulse based on optical photon transport and a PMT response function. The photon transport was calculated using Geant4 Monte Carlo code and the response function with a BC408 organic scintillator. The obtained percentage RMS value of the difference between the measured and simulated pulse with suitable scintillation properties using GSO:Ce (0.4, 1.0, 1.5 mol%), $LaBr_3$:Ce and BGO scintillators were 2.41%, 2.58%, 2.16%, 2.01%, and 3.32%, respectively. The proposed technique demonstrates high reproducibility of the measured pulse and can be applied to simulation studies of various radiation measurements. © *2016 Author(s). All article content, except where otherwise noted, is licensed under a Creative Commons Attribution (CC BY) license (http://creativecommons.org/licenses/by/4.0/).* [http://dx.doi.org/10.1063/1.4959186]

I. INTRODUCTION

In radiation measurements the signal pulse generated from a radiation detector is the most fundamental information of incident radiation. Signal pulses are sent to signal processing devices (i.e., discriminator or multi-channel analyzer) with a measurement objective. Particularly, the signal pulse shape is important for pulse shape discrimination (PSD) analysis which aims to improve the measurement accuracy such as energy resolution[1] or background rejection using particle identification.[2,3] The difference in emission properties of scintillation fluorescence caused by an incident particle type could be detected by PSD analysis.[3–7] Similarly, gamma-neutron discrimination by a zero crossing time method is a well-known technique using an organic scintillator in a mixed radiation field.[4,5] Other PSD techniques (i.e., charge comparison method[6,7] or peak-to-charge discrimination (PQD) method with $LaBr_3$:Ce scintillator[8]) have also been developed for precise signal separation using various scintillators. Recently, PSD analysis has been applied for a depth-of-interaction (DOI) detector in a small positron emission tomography (PET) device aiming at the improvement of image quality.[9] The DOI detector consists of a multi-layered scintillator with different scintillation properties.[10,11] Moreover, a phoswich (phosphor sandwich) detector which consists of a few scintillators identifies an incident particle type by PSD analysis in a common readout,[12] and applies a background rejection method using anti-Compton analysis.[13] To evaluate the PSD performance with various detectors, it is essential that the pulse emulation reproduces the exact measured pulse. To the best of our knowledge, the emulation techniques for PMT anode pulse with high accuracy have not yet been developed, since the anode pulse consists of quite complex components.

Scintillation light pulses are generally converted to electric pulses using a photo-electric converter (i.e., photomultiplier tube (PMT) or photodiode). The scintillation light is transported to a PMT photocathode surface from an emission point through a process of complex reflection and refraction in the scintillation crystal and a reflector.[14] The decay curve of the emission and arriving time distribution at the PMT photocathode are different, since a time deviation is added to the emission decay curve in the transport process. The time deviation is considered to be a very complex quantity because it depends on the crystal structure, surface condition, and optical properties of the scintillator. Additionally, the electron transit time spread increases during electron amplification in the PMT.[15] As a result, the PMT anode pulse is spread in the time domain in comparison with the arriving time distribution at the PMT photocathode. A circuit constant of HV divider equipped with the PMT also affects the PMT anode pulse shape. Thus, the arriving time distribution at the PMT photocathode and the PMT response function is required to reproduce the exact measured pulse.

In the present method, in order to achieve the arriving time distribution at the PMT photocathode, the scintillation process and optical photon transport were calculated using the Geant4 Monte Carlo code.[16,17] To simulate the optical photon transport calculation in Geant4, a material surface model was implemented known as DETECT2000.[18]

In this study, the accuracy of pulse reproducibility was evaluated using pulses of GSO:Ce (0.4, 1.0, 1.5 mol%), $LaBr_3$:Ce, and BGO scintillators equipped with a R6231-100 PMT. We report the procedure of the proposed pulse emulation technique and its accuracy.

a)Electronic mail: masayori@med.hokudai.ac.jp

 © Author(s) 2016.

Reuse of AIP Publishing content is subject to the terms at: https://publishing.aip.org/authors/rights-and-permissions. Download to IP: 133.87.84.66 On: Tue, 02 Aug 2016 05:42:11

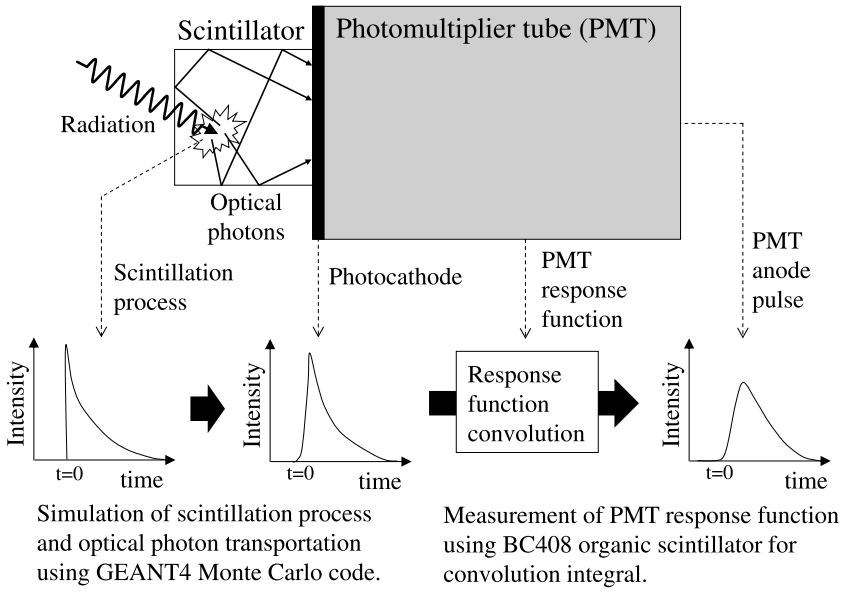

FIG. 1. Schematic diagram of the present pulse emulation method.

II. MATERIAL AND METHOD

A. Theory of pulse emulation for scintillation detectors

Figure 1 shows the present method based on the Geant4.9.5 Monte Carlo simulation and the measurement of the PMT response function. To obtain the arriving time distribution at the PMT photocathode, a scintillation process and an optical photon transport were calculated using the Geant4 Monte Carlo code. The PMT response function was measured using a BC408 organic scintillator which has fast scintillation properties. The simulated pulse was obtained by a convolution integral of the PMT photocathode arriving time and the PMT response function.

B. Measurement system

In the present method, an anode pulse of the PMT (R6231-100, Hamamatsu Photonics) equipped with a divider circuit (E1198-26 MOD, Hamamatsu Photonics) was measured directly using a digital oscilloscope (WaveRunner 64xi, LeCroy, 5 GS/s, band width 600 MHz).[8] This helps to avoid signal distortion from electric devices such as a shaping amplifier. This system was used for the measurement of the PMT response function and for the accuracy assessment of the present method as well.

C. Scintillation detectors

In this study, five different scintillators, GSO:Ce (Gd_2SiO_5, Ce 0.4, 1.5, 1.0 mol%, Hitachi Chemical/OXIDE), $LaBr_3$:Ce (Ce 5.0 mol%, B308, BrilLanCe^{TM}, Saint-Gobain), and BGO ($Bi_4Ge_5O_{12}$, Saint-Gobain) were used for the evaluation of pulse reproduction accuracy. Additionally, the BC408 organic scintillator (Saint-Gobain) was used for the measurement of the PMT response function. Published scintillation properties for these scintillators are listed in Table I.[18–25] As shown in Figure 2, the structure of the GSO:Ce scintillators is $\Phi 0.9'' \times 1.0''$ (Ce 0.4 mol%), $2.5 \times 2.5 \times 25$ mm^3 (Ce 1.0 mol%), and $\Phi 12$ mm $\times$ 12 mm (Ce 1.5 mol%). The $LaBr_3$:Ce scintillator is a cylinder shape of $\Phi 1.5'' \times 1.5''$, BGO and BC408 scintillators are rectangle shape of $12 \times 14 \times 2$ mm^3 and $20 \times 20 \times 1$ mm^3,

TABLE I. Material properties of GSO:Ce (0.4, 1.0, 1.5 mol%), $LaBr_3$:Ce, BGO, and BC408 scintillator.

Scintillator	Density (g/cm^3)	Wavelength (nm)[a]	Refractive index[a]	Photon yield (photons/MeV)	Rise (ns)	Decay (ns)
GSO:Ce						70(90%)
0.4 mol%						650(10%)
GSO:Ce	6.71	435	1.87	9 000	10	40(90%)
1.0 mol%						418(10%)
GSO:Ce						32(90%)
1.5 mol%						307(10%)
$LaBr_3$:Ce	5.08	380	1.9	63 000	0.93	16
BGO	7.13	480	2.15	8 000	2.8	60(10%)
						300(90%)
BC408	1.032	425	1.58	10 000	0.9	2.1 (Pulse width 2.5)

[a]Peak emission.

Reuse of AIP Publishing content is subject to the terms at: https://publishing.aip.org/authors/rights-and-permissions. Download to IP: 133.87.84.66 On: Tue, 02 Aug 2016 05:42:11

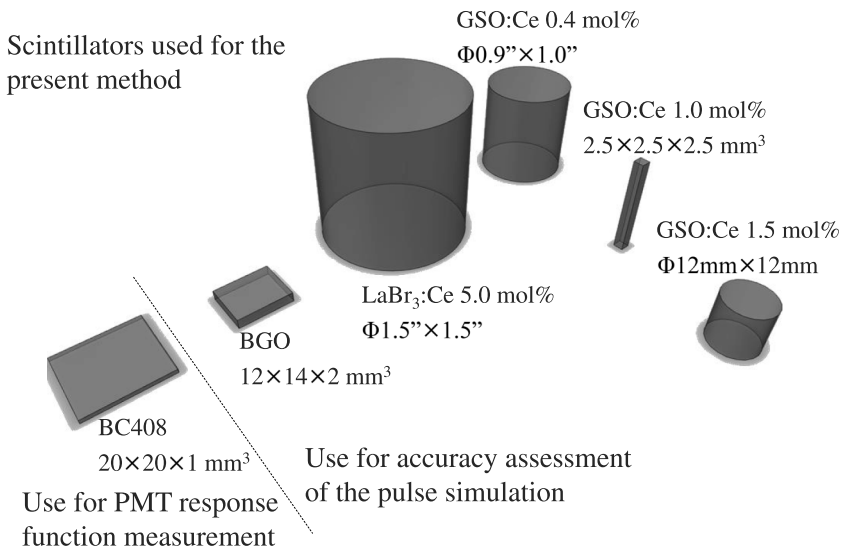

FIG. 2. Structures of GSO:Ce (0.4, 1.0, 1.5 mol%), $LaBr_3$:Ce, BGO, and BC408 scintillators.

respectively. The widest flat face of the scintillators was connected to the PMT photocathode using optical grease (BC630, Saint-Gobain). These scintillators were wrapped with PTFE reflector tape (BC642, Saint-Gobain) except the face connected to the PMT photocathode.

D. Optical tracking simulation

In the current work, both the scintillation process and Cerenkov process were included. Cerenkov photons produced in each wavelength were obtained by the theoretical formula which is a function of refractive index of the material and charged particle energy. Scintillation properties of GSO:Ce (Ce 0.4, 1.0, 1.5 mol%),[18–20] $LaBr_3$:Ce,[21–23] and BGO[24,25] scintillators were reproduced from published data. The envelope function with $f(t) = \exp(-t/\tau_D)$ and $g(t) = (1 - \exp(-t/\tau_R))$ (τ_D and τ_R are decay and rise time constant, respectively) was used for the emission decay curve in the Geant4.9.5 Monte Carlo code. In this simulation, an optical surface model between the scintillator and reflector was ground back painted with specular lobe coefficient 1.0, since this model is recommended for the exact reproducibility of the real surface.[17] Additionally, the quantum efficiency of the PMT photocathode surface was included as a nominal value. Photons were generated by irradiation from an external ^{137}Cs gamma-ray source. We calculated time profiles of the scintillation emission and the arriving time at the PMT photocathode using GSO:Ce (Ce 0.4, 1.0, 1.5 mol%), $LaBr_3$:Ce, and BGO scintillators. For the convolution of the PMT response function, the sampling rate of the arriving time at the PMT photocathode was calculated with 2.5 ns. For the accuracy assessment of the simulated pulse, average pulses of 100 simulation data were used.

E. Estimation of PMT response function

The PMT response function is difficult to estimate by simulation because of the complex behavior of transit electrons in a PMT which directly affects the PMT response function. Generally, to obtain the PMT response function, a PMT photocathode is irradiated directly with a fast pulsed laser.[15] Instead of a fast pulsed laser, a BC408 organic scintillator was used to obtain the PMT response function with a ^{137}Cs gamma-ray source (235.4 kBq). BC408 has fast scintillation properties with 2.5 ns pulse width. The luminous time of BC408 was assumed to be a 2.5 ns square pulse. The PMT anode pulse of the BC408 scintillator could therefore be assumed to be the PMT response function. The PMT response function was obtained from the average of 100 pulses using events of the same energy deposition. However, the PMT response function measured by the oscilloscope had a sampling rate of 0.2 ns (5 GS/s); thus, the sampling rate of the PMT response function was converted to 2.5 ns from 0.2 ns using a cubic spline interpolation for the convolution integral.

We obtained two response functions with supplied voltages of 1000 V and 1300 V. GSO:Ce (Ce 0.4, 1.5, 1.0 mol%) and $LaBr_3$:Ce scintillators were used at 1000 V and BGO scintillator at 1300 V. In the case of BGO and GSO:Ce scintillators, the PMT and divider circuit were shared with the measurements of the PMT response function. However, the PMT and divider circuit of the $LaBr_3$:Ce scintillator were different with the same type of material because the crystal and PMT could not be separated in combined products.

F. Validation of pulse-shape reproducibility

To obtain a simulated pulse, the PMT response functions were convoluted to the arriving time distribution at the PMT photocathode as shown in Fig. 1. To estimate the difference between the measured and the simulated pulse, the sampling rate of the simulated pulse was converted to 0.2 ns from 2.5 ns using a cubic spline interpolation.

The supplied PMT voltage was adjusted to 1000 V for the GSO:Ce and $LaBr_3$:Ce scintillators, and 1300 V for the BGO scintillator to obtain sufficient signal while avoiding signal saturation. The pulse signals from the scintillators were measured with the oscilloscope with an external ^{137}Cs radiation source (235.4 kBq). The energy spectrum was

Reuse of AIP Publishing content is subject to the terms at: https://publishing.aip.org/authors/rights-and-permissions. Download to IP: 133.87.84.66 On: Tue, 02 Aug 2016 05:42:11

obtained by integrating the pulse signal, which is equivalent to signal charge, using an in-house code. For the analysis, we averaged 100 pulses at 662 keV total absorption peak.

We quantified the accuracy of reproducibility for the simulated signal pulse as a percentage root mean square (RMS) of the difference between the measured and the simulated pulse within a range of measured pulse intensity >10% of the peak value. However, the percentage RMS value depends significantly on the normalized point in the time domain; therefore, we optimized the normalized point in order to obtain the minimum percentage RMS value. Additionally, we compared the integrated charge of the measured and the simulated pulse for the accuracy assessment.

III. RESULT

A. Simulation of optical photon tracking

Figures 3(a.1,2)–3(e.1,2) shows the time profile of the emission decay curve and the PMT photocathode arriving time calculated by Geant4 Monte Carlo simulation using GSO:Ce (0.4, 1.0, 1.5 mol%), $LaBr_3$:Ce, and BGO scintillators. The sampling rate of Figs. 3(a.2)–3(e.2) was calculated to be 0.2 ns in order to maximize the rising edge of the pulses. The contribution of the photons produced by the Cerenkov process was less than 1% in all scintillators. It is difficult to differentiate between the emission decay curve and the arriving time at the PMT photocathode using small crystal structures such as GSO:Ce 1.0 mol% and BGO scintillators. We found the maximum difference using the $LaBr_3$:Ce scintillator which was the largest structure in this study.

The signal deviation was determined by the photon yield with intensity ratio of fast and slow components in the simulation. Therefore, the signal deviation of the $LaBr_3$:Ce scintillator which has a large photon yield was obtained with much lower value than the other scintillators. A large deviation of GSO:Ce (Ce 0.4, 1.0, 1.5 mol%) in a range of >200 ns was due to a lower photon yield caused by the 10% slow component.

B. Measurement of PMT response function

The response functions of R6231-100 PMT with supplied voltages of 1000 V and 1300 V were obtained by using a BC408 scintillator with external ^{137}Cs radiation source as shown in Figure 4. The pulse shape normalized with a peak value was unchanged in the energy spectrum using constant supplied voltage. Figure 4 shows that the PMT response function of 1000 V spread slightly more than that of 1300 V, since the electron transit time spread in the PMT is in inverse relation with the supplied voltage.[15]

C. Validation of pulse-shape reproducibility

Figures 5-7(a) show the energy spectra obtained by the integrated charge of pulses acquired with the oscilloscope

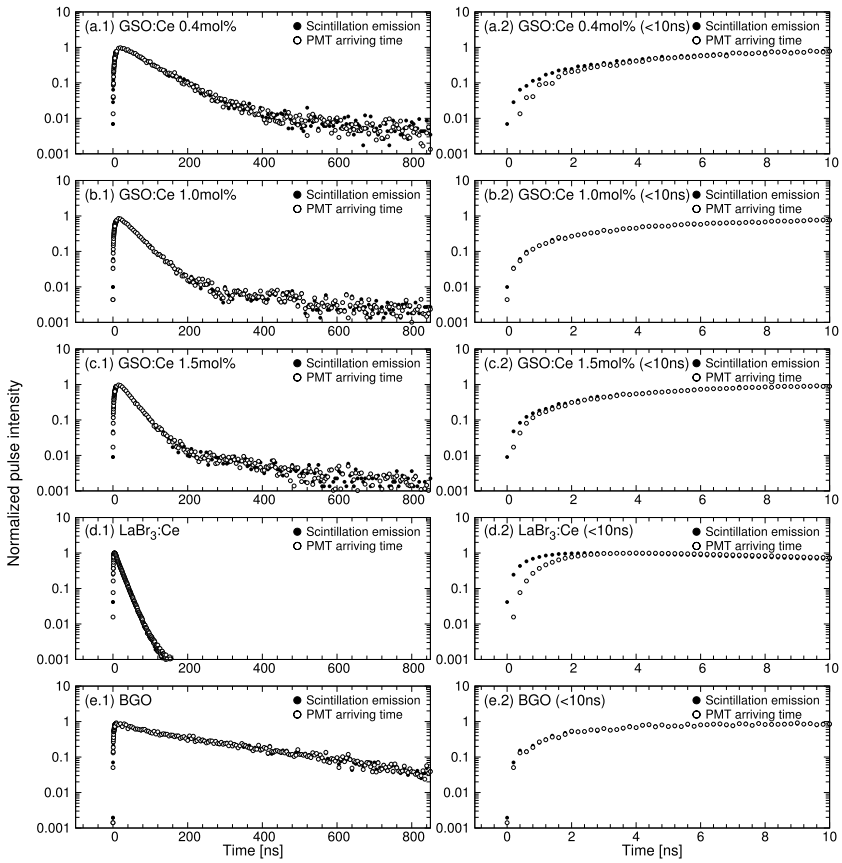

FIG. 3. Emission decay curve and PMT photocathode arriving time simulated by Geant4 Monte Carlo code using GSO:Ce (a.1) 0.4 mol%, (b.1) 1.0 mol%, (c.1) 1.5 mol%, (d.1) $LaBr_3$:Ce, and (e.1) BGO scintillators. (a.2)–(e.2) shown an expansion of the rising edge (<10 ns) in each scintillator.

Reuse of AIP Publishing content is subject to the terms at: https://publishing.aip.org/authors/rights-and-permissions. Download to IP: 133.87.84.66 On: Tue, 02 Aug 2016 05:42:11

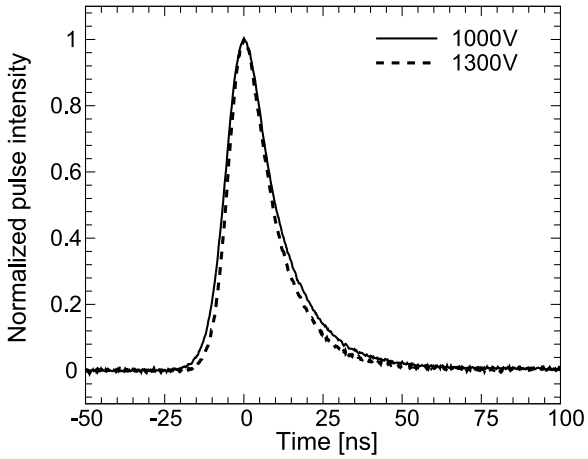

FIG. 4. Response function of the R6231-100 PMT measured by BC408 organic scintillator at supplied voltage of 1300 V and 1000 V.

using GSO:Ce (0.4, 1.0, 1.5 mol%), $LaBr_3$:Ce, and BGO scintillators. The peak to Compton ratio of energy spectrum depends on the crystal structure, its density, and energy resolution. A lower threshold level of these spectra was determined by a rising edge trigger level of the oscilloscope. Energy resolution estimated by a fitting analysis with a gauss function was 10.8%, 14.1%, 9.79% (GSO:Ce 0.4, 1.0, 1.5 mol%), 3.36% ($LaBr_3$:Ce), and 13.1% (BGO) using full width at half-maximum (FWHM) at total absorption peak (662 keV). The comparison between the measured and the simulated pulses of GSO:Ce (0.4, 1.0, 1.5 mol%), $LaBr_3$:Ce, and BGO scintillators with the optimization of a normalized point in a time domain are shown in Figures 5(a)-5(c), Figures 6(b) and 7(b), respectively. The accuracy of the pulse reproducibility was assessed by the percentage RMS value of difference between measured and simulated pulse as shown in Table II. The difference in the integrated charge is also summarized in Table II.

1. GSO:Ce (0.4, 1.0, 1.5 mol%) scintillators

Scintillation properties of a GSO:Ce scintillator depend on a dopant concentration as shown in Figs. 5(b)-5(d). The percentage RMS value for the GSO:Ce (0.4, 1.0, 1.5 mol%) scintillators were 3.60%, 2.60%, 10.6% and the difference in the integrated charge wsa 4.93%, 3.37%, 16.75%, respectively. The simulated pulses for the GSO:Ce 0.4, 1.0 mol% scintillators were reproduced almost the same as the measured pulse except for the range of 120-300 ns. However, the simulated pulse shape of the GSO:Ce 1.5 mol% scintillator shows relatively large difference from the measured pulse as shown in Fig. 5(d). The difference in the integrated charge and the percentage RMS value indicate a similar tendency as shown in Table II.

2. $LaBr_3$ scintillator

The $LaBr_3$:Ce scintillator performed with excellent energy resolution and fast signal response as shown in Figs. 6(a) and 6(b). Moreover, we obtained the highest accuracy of pulse reproducibility, the percentage RMS value of 2.41%, and a difference in integrated charge of −2.09% as shown in Table II. Even though the PMT and the divider circuit of the $LaBr_3$:Ce scintillator were different from the device of the PMT response function measurement, a high accuracy of pulse reproducibility was achieved.

3. BGO scintillator

A percentage RMS value of 4.75% and a difference in the integrated charge of 4.25% were obtained using the BGO scintillator as shown in Table II. A difference between the measured and the simulated pulse was observed in the signal rise region (Fig. 7(b)). On the other hand, the simulated pulse shape of the signal decay region reproduced the exact measured pulse.

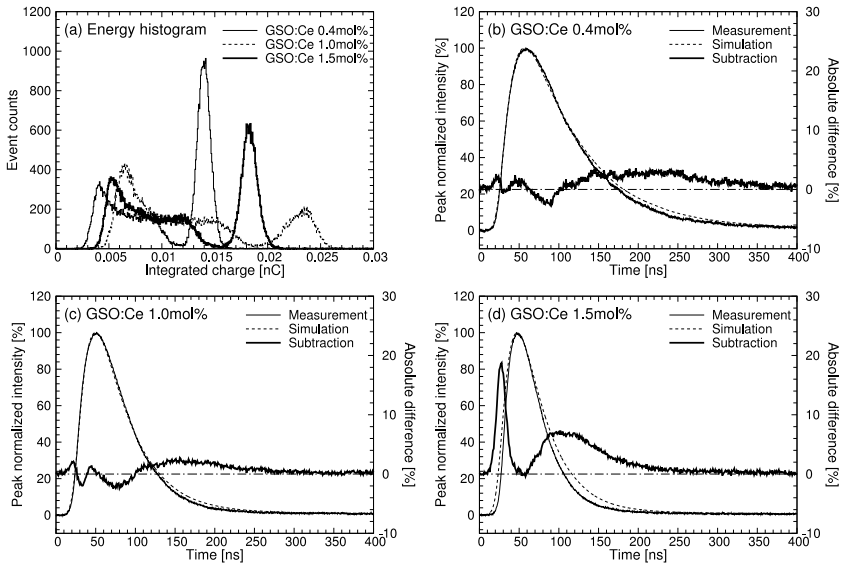

FIG. 5. (a) Energy spectra using GSO:Ce (0.4, 1.0, 1.5 mol%) scintillators with external radiation source ^{137}Cs. Difference between the measured and simulated pulses using the present method with GSO:Ce scintillators with Ce concentration of (b) 0.4 mol%, (c) 1.0 mol%, (d) 1.5 mol%.

Reuse of AIP Publishing content is subject to the terms at: https://publishing.aip.org/authors/rights-and-permissions. Download to IP: 133.87.84.66 On: Tue, 02 Aug 2016 05:42:11

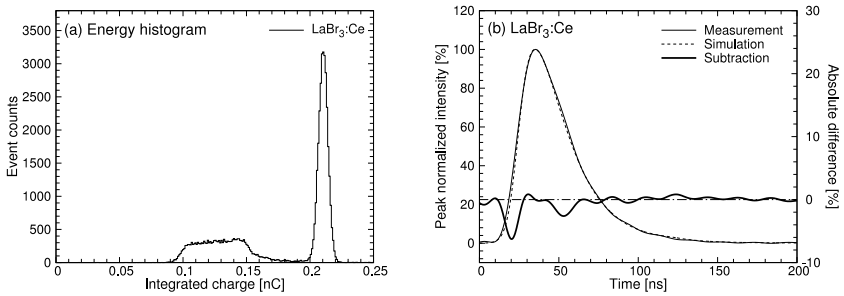

FIG. 6. (a) Energy spectrum using $LaBr_3$:Ce scintillator with external radiation source ^{137}Cs. (b) Difference between the measured and simulated pulses using the present method with a $LaBr_3$:Ce scintillator.

IV. DISCUSSION

A. Accuracy of pulse reproducibility

Fig. 5(d) shows that sufficient accuracy of pulse reproduction was not achieved using the GSO:Ce 1.5 mol% scintillator. Similarly, Figs. 5(b) and 5(c) indicate a slight difference between the measured and the simulated pulse using GSO:Ce 0.4, 1.0 mol% scintillators. This suggests that the preset scintillation properties were not precise in the Geant4 Monte Carlo simulation, since the Ce concentration, which determines the scintillation properties, depends on the fraction of melt solidification in the crystal ingot grown by the Czochralski technique.[26,27] Moreover, the gradient of the Ce concentration in the crystal ingot increases with the amount of CeO_2 in the starting material.[28] Therefore, we tried to estimate the scintillation properties of GSO:Ce (0.4, 1.0, 1.5 mol%) scintillators for the exact measured pulse reproduction. The estimated parameters using GSO:Ce scintillators improved the accuracy of pulse reproduction as shown in Figures 8(a)-8(c) and Table II. It seems that the GSO:Ce scintillators used in the present method have a higher Ce concentration than the nominal value, since the decay time constant and Ce concentration are in inverse relation. For the present pulse emulation method using scintillators grown by the Czochralski technique, it is recommended to use precise scintillation properties obtained by measurements rather than the nominal value.

To improve the pulse reproducibility of $LaBr_3$:Ce scintillators, we estimated a suitable decay time constant as shown in Table II. As a result, the difference in the integrated charge of simulated pulse with estimated time constant is quite smaller than the simulated pulse with nominal time constant. The sufficient accuracy of pulse reproducibility using the $LaBr_3$:Ce scintillator was obtained with a nominal decay constant, but it was also possible to improve the pulse reproducibility with an estimated decay constant.

According to previous research, light collection time due to the scintillator volume might affect the rise time.[24] Moreover, the scintillation time properties of the BGO scintillator strongly depend on the temperature.[29] Thus, the time constant of the BGO scintillator is estimated to reproduce the exact measured pulse. The estimated parameters of the BGO scintillator which reproduced accurately the measured pulse are shown in Fig. 8(d) and Table II.

Precise emission decay curves for the GSO:Ce and BGO scintillators are more difficult to reproduce than for the $LaBr_3$:Ce scintillator, since the scintillation time properties of the GSO:Ce and BGO scintillators have two major decay constants. Moreover the properties vary due to several reasons. However, high accuracy pulse reproduction with the nominal scintillation properties was obtained except for the crystals with large dopant concentrations such as the GSO:Ce 1.5 mol%.

B. Limitation of the PMT response function measured by the BC408

In the present method, the PMT response function was obtained using a BC408 organic scintillator which is assumed to have a square pulse of 2.5 ns. However, the luminous time structure of BC408 is actually based on its scintillation properties. It is considered that the accuracy of pulse reproducibility is reduced by the luminous time structure of the BC408 scintillator. Particularly, the accuracy reduction occurred in the case of a scintillator with fast time properties

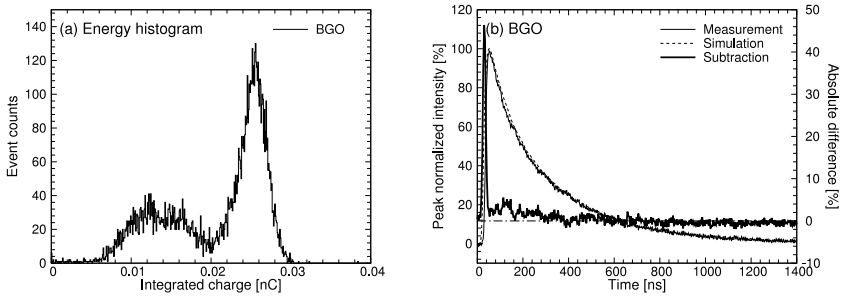

FIG. 7. (a) Energy spectrum using BGO scintillator with ^{137}Cs external radiation source. (b) Difference between the measured and simulated pulses using the present method with a BGO scintillator.

Reuse of AIP Publishing content is subject to the terms at: https://publishing.aip.org/authors/rights-and-permissions. Download to IP: 133.87.84.66 On: Tue, 02 Aug 2016 05:42:11

TABLE II. Results of the accuracy assessment of the pulse reproduction and parameter estimation for accuracy improvement using GSO:Ce 0.4, 1.0, 1.5 mol%, $LaBr_3$:Ce, and BGO scintillators.

	Nominal time constant				Estimated time constant			
Scintillators	Rise (ns)	Decay (ns)	RMS (%)	$\delta Q/Q_{meas.}(\%)$[a]	Rise (ns)	Decay (ns)	RMS (%)	$\delta Q/Q_{meas.}(\%)$[a]
GSO:Ce	10	70(90%)	3.65 ± 0.38	4.93 ± 0.18	10	65(90%)	2.41 ± 0.25	−0.11 ± 0.18
0.4 mol%		650(10%)				650(10%)		
GSO:Ce	10	40(90%)	2.60 ± 0.16	3.37 ± 0.17	10.5	38(90%)	2.58 ± 0.1	0.55 ± 0.17
1.0 mol%		418(10%)				400(10%)		
GSO:Ce	10	32(90%)	10.6 ± 0.69	16.7 ± 0.18	7	26(90%)	2.16 ± 0.14	0.85 ± 0.17
1.5 mol%		307(10%)				215(10%)		
$LaBr_3$:Ce	0.98	16	2.41 ± 0.06	−2.09 ± 0.11	0.98	17.2	2.01 ± 0.05	0.18 ± 0.11
BGO	2.8	60(10%)	5.41 ± 0.11	4.24 ± 0.31	1.5	50(10%)	3.32 ± 0.68	0.67 ± 0.30
		300(90%)				300(90%)		

[a] $\delta Q = Q_{meas.} - Q_{sim.}$.

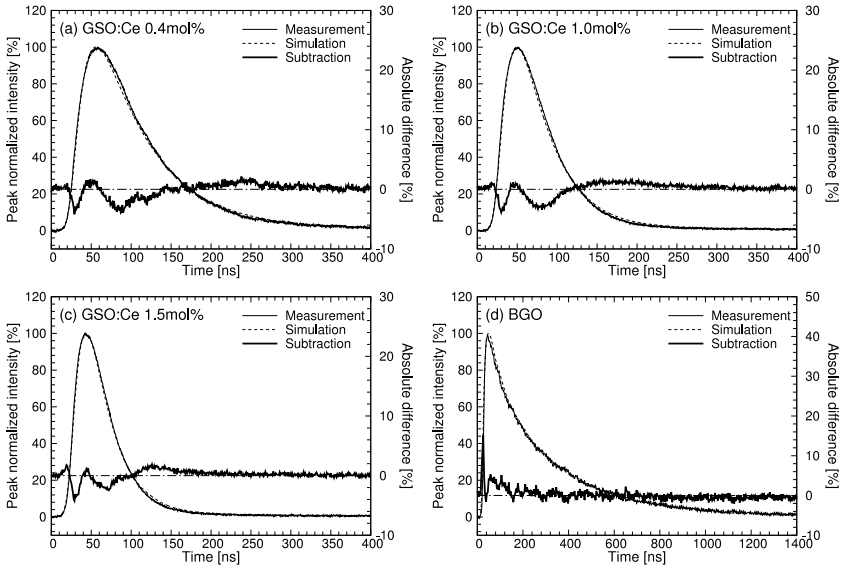

FIG. 8. The measured pulse and the simulated pulse of GSO:Ce (a) 0.4 mol%, (b) 1.0 mol%, (c) 1.5 mol%, (d) BGO scintillators with the estimated decay constant.

such as an organic scintillator in the present method. However, the simulated pulse of the $LaBr_3$:Ce scintillator, which has a short decay time constant of 16 ns in inorganic scintillators, reproduced the exact measured pulse as shown in Fig. 6(b). This means that the measurement of the PMT response function using the BC408 scintillator can be applied to the present pulse simulation of various inorganic scintillators.

C. Extensibility of the present method

The present method can be applied to a simulation study of radiation measurements using a scintillator equipped with a PMT, particularly for the estimation of an optimized scintillator and performance evaluation for PSD analysis. Moreover, a simulation of a subsequent circuit of a PMT can be achieved by combining a SPICE simulation and the current method. Recently, development of an avalanche photodiode (APD) has been considered as a subsequent device coupled with a scintillator. In the future, we are planning to investigate the accuracy of pulse reproducibility with an APD device using the present simulation method.

V. CONCLUSION

We have developed a novel emulation method for a PMT anode pulse with sufficient accuracy. The accuracy of pulse reproducibility was demonstrated by using various scintillators. The authors believe that the present method will be used as one of the standard techniques for a simulation study using a scintillator equipped with a PMT.

ACKNOWLEDGMENTS

The authors would like to express deep gratitude to Hitachi Chemical/OXIDE for providing GSO:Ce (0.4, 1.5 mol%) scintillators for long time, and gratefully acknowledge the Graduate School of Health Science, Hokkaido University for facilitating experiment facilities and external radiation sources.

[1]L. Jones and P. Woollam, "Resolution improvement in CdTe gamma detectors using pulse-shape discrimination," Nucl. Instrum. Methods **124**, 591–595 (1975).
[2]C. Ammerlaan, R. Rumphorst, and L. Koerts, "Particle identification by pulse shape discrimination in the p-i-n type semiconductor detector," Nucl. Instrum. Methods **22**, 189–200 (1963).

Reuse of AIP Publishing content is subject to the terms at: https://publishing.aip.org/authors/rights-and-permissions. Download to IP: 133.87.84.66 On: Tue, 02 Aug 2016 05:42:11

[3]C. Bartle, "A study of (n,p) and (n,a) reactions in NaI(Tl) using a pulse-shape-discrimination method," Nucl. Instrum. Methods **124**, 547–550 (1975).
[4]R. Winyard, J. Lutkin, and G. McBeth, "Pulse shape discrimination in inorganic and organic scintillators. I," Nucl. Instrum. Methods **95**, 141–153 (1971).
[5]R. Winyard and G. McBeth, "Pulse shape discrimination in inorganic and organic scintillators. II," Nucl. Instrum. Methods **98**, 525–533 (1972).
[6]L. Giacomelli, A. Zimbal, M. Reginatto, and K. Tittelmeier, "Evaluation of a digital data acquisition system and optimization of n-g discrimination for a compact neutron spectrometer," Rev. Sci. Instrum. **82**, 013505 (2011).
[7]K. Ishii, K. Shinohara, M. Ishikawa, M. Baba, M. Isobe, A. Okamoto, S. Kitajima, and M. Sasao, "Fast neutron-gamma discrimination on neutron emission profile measurement on JT-60U," Rev. Sci. Instrum. **81**, 10D334 (2010).
[8]R. Ogawara and M. Ishikawa, "Feasibility study on signal separation for spontaneous alpha decay in $LaBr_3$:Ce scintillator by signal peak-to-charge discrimination," Rev. Sci. Instrum. **86**, 085108 (2015).
[9]T. Yamaya, E. Yoshida, T. Inaniwa, S. Sato, Y. Nakajima, H. Wakizaka, D. Kokuryo, A. Tsuji, T. Mitsuhashi, H. Kawai, H. Tashima, F. Nishikido, N. Inadama, H. Murayama, H. Haneishi, M. Suga, and S. Kinouchi, "Development of a small prototype for a proof-of-concept of openpet imaging," Phys. Med. Biol. **56**, 1123 (2011).
[10]A. Saoudi, C. M. Pepin, F. Dion, M. Bentourkia, R. Lecomte, M. Andreaco, M. Casey, R. Nutt, and H. Dautet, "Investigation of depth-of-interaction by pulse shape discrimination in multicrystal detectors read out by avalanche photodiodes," IEEE Trans. Nucl. Sci. **46**, 462–467 (1999).
[11]N. Inadama, H. Murayama, T. Omura, T. Yamashita, S. Yamamoto, H. Ishibashi, H. Kawai, K. Omi, T. Umehara, and T. Kasahara, "A depth of interaction detector for PET with GSO crystals doped with different amounts of Ce," IEEE Trans. Nucl. Sci. **49**, 629–633 (2002).
[12]J. Alarja, A. Dauchy, A. Giorni, C. Morand, E. Pollaco, P. Stassi, R. Billerey, B. Chambon, B. Cheynis, D. Drain, and C. Pastor, "Charged particles identification with a CsI(Tl) scintillator," Nucl. Instrum. Methods Phys. Res., Sect. A **242**, 352–354 (1986).
[13]A. T. Farsoni, B. Alemayehu, A. Alhawsawi, and E. M. Becker, "A compton-suppressed phoswich detector for gamma spectroscopy," J. Radioanal. Nucl. Chem. **296**, 63–68 (2012).
[14]Y. Xiaoguang, "A study of light collection efficiency in scintillation detectors," Nucl. Instrum. Methods Phys. Res., Sect. A **228**, 101–104 (1984).
[15]H. Kyushima, Y. Hasegawa, A. Atsumi, K. Nagura, H. Yokota, M. Ito, J. Takeuchi, K. Oba, H. Matsuura, and S. Suzuki, "Photomultiplier tube of new dynode configuration," IEEE Trans. Nucl. Sci. **41**, 725–729 (1994).
[16]J. Allison, K. Amako, J. Apostolakis, H. Araujo, P. A. Dubois, M. Asai, G. Barrand, R. Capra, S. Chauvie, R. Chytracek, G. A. P. Cirrone, G. Cooperman, G. Cosmo, G. Cuttone, G. G. Daquino, M. Donszelmann, M. Dressel, G. Folger, F. Foppiano, J. Generowicz, V. Grichine, S. Guatelli, P. Gumplinger, A. Heikkinen, I. Hrivnacova, A. Howard, S. Incerti, V. Ivanchenko, T. Johnson, F. Jones, T. Koi, R. Kokoulin, M. Kossov, H. Kurashige, V. Lara, S. Larsson, F. Lei, O. Link, F. Longo, M. Maire, A. Mantero, B. Mascialino, I. McLaren, P. M. Lorenzo, K. Minamimoto, K. Murakami, P. Nieminen, L. Pandola, S. Parlati, L. Peralta, J. Perl, A. Pfeiffer, M. G. Pia, A. Ribon, P. Rodrigues, G. Russo, S. Sadilov, G. Santin, T. Sasaki, D. Smith, N. Starkov, S. Tanaka, E. Tcherniaev, B. Tome, A. Trindade, P. Truscott, L. Urban, M. Verderi, A. Walkden, J. P. Wellisch, D. C. Williams, D. Wright, and H. Yoshida, "Geant4 developments and applications," IEEE Trans. Nucl. Sci. **53**, 270–278 (2006).
[17]A. Levin and C. Moisan, "A more physical approach to model the surface treatment of scintillation counters and its implementation into detect," in *IEEE Nuclear Science Symposium Conference Record* (IEEE, 1996), Vol. 2, pp. 702–706.
[18]C. L. Melcher, J. S. Schweitzer, T. Utsu, and S. Akiyama, "Scintillation properties of GSO," IEEE Trans. Nucl. Sci. **37**, 161–164 (1990).
[19]S. Shimizu, K. Sumiya, H. Ishibashi, N. Senguttvan, B. S. Redkin, M. Ishii, M. Kobayashi, K. Susa, and H. Murayama, "Effect of Mg, Zr, Ta—Doping on scintillation properties of Gd_2SiO_5:Ce crystal," in *IEEE Nuclear Science Symposium Conference Record* (IEEE, 2002), Vol. 1, pp. 96–100.
[20]Q.-Z. Zhao, J.-R. Qiu, C.-J. Zhao, X.-W. Jiang, C.-S. Zhu, and G.-J. Zhao, "Investigation of optical properties of Ce^{3+}-doped Gd_2SiO_5 crystal irradiated by a femtosecond laser," Opt. Commun. **255**, 97–101 (2005).
[21]H. T. van Dam, S. Seifert, W. Drozdowski, P. Dorenbos, and D. R. Schaart, "Optical absorption length, scattering length, and refractive index of $LaBr_3$:Ce^{3+}," IEEE Trans. Nucl. Sci. **59**, 656–664 (2012).
[22]A. Iltis, M. Mayhugh, P. Menge, C. Rozsa, O. Selles, and V. Solovyev, in *TRDs for the Third Millenium Proceedings of the 3rd Workshop on Advanced Transition Radiation Detectors for Accelerators and Space Applications* ["Lanthanum halide scintillators: Properties and applications," Nucl. Instrum. Methods Phys. Res., Sect. A **563**, 359–363 (2006)].
[23]J. Glodo, W. W. Moses, W. M. Higgins, E. V. D. van Loef, P. Wong, S. E. Derenzo, M. J. Weber, and K. S. Shah, "Effects of Ce concentration on scintillation properties of $LaBr_3$:Ce," IEEE Trans. Nucl. Sci. **52**, 1805–1808 (2005).
[24]M. Moszynski, C. Gresset, J. Vacher, and R. Odru, "Timing properties of BGO scintillator," Nucl. Instrum. Methods Phys. Res. **188**, 403–409 (1981).
[25]D. F. Anderson, "Properties of the high-density scintillator cerium fluoride," IEEE Trans. Nucl. Sci. **36**, 137–140 (1989).
[26]G. Loutts, A. Zagumennyi, S. Lavrishchev, Y. Zavartsev, and P. Studenikin, "Czochralski growth and characterization of $(Lu_{1-x}Gd_x)_2SiO_5$ single crystals for scintillators," J. Cryst. Growth **174**, 331–336 (1997), American Crystal Growth 1996 and Vapor Growth and Epitaxy 1996.
[27]K. Kurashige, A. Gunji, M. Kamada, N. Shimura, H. Ishibashi, K. Yoshida, N. Senguttuvan, K. Sumiya, S. Shimizu, and H. Murayama, "Large GSO single crystals with a diameter of 100 mm and their scintillation performance," IEEE Trans. Nucl. Sci. **51**, 742–745 (2004).
[28]H. Ishibashi, K. Kurashige, Y. Kurata, K. Susa, M. Kobayashi, M. Tanaka, K. Hara, and M. Ishii, "Scintillation performance of large Ce-doped Gd_2SiO_5 (GSO) single crystal," IEEE Trans. Nucl. Sci. **45**, 518–521 (1998).
[29]C. L. Melcher, J. S. Schweitzer, A. Liberman, and J. Simonetti, "Temperature dependence of fluorescence decay time and emission spectrum of bismuth germanate," IEEE Trans. Nucl. Sci. **32**, 529–532 (1985).

Reuse of AIP Publishing content is subject to the terms at: https://publishing.aip.org/authors/rights-and-permissions. Download to IP: 133.87.84.66 On: Tue, 02 Aug 2016 05:42:11